Volume 1 | Number 1 | Jan 2013 | Pages 1–100

Journal of
Materials Chemistry A

Materials for energy and sustainability
www.rsc.org/materialsA

ROYAL SOCIETY
OF CHEMISTRY

ROYAL SOCIETY
OF CHEMISTRY

www.rsc.org/materialsA

Journal Name

ARTICLE

Metal–organic frameworks: A new promising class of material for high performance supercapacitor electrode

Jie Yang,[a,b] Peixun Xiong, [a,b] Cheng Zheng, [a,b] Heyuan Qiu, [a,b] and Mingdeng Wei [a,b]

A layered structure Ni-based MOF was synthesized and, for the first time, was used as the electrode material for a supercapacitor. It exhibited large specific capacitance, high rate capability and cycling stability. Capacitances of 1127 and 668 F g^{-1} can be achieved at rates of 0.5 and 10 A g^{-1}, respectively. At the same time, over 90% performance was retained after 3000 cycles. These excellent electrochemical properties may be related to the intrinsic characteristics of Ni-based MOF materials.

Introduction

Supercapacitors have been regarded as one of the most promising energy storage devices because their higher energy densities are orders of magnitude higher than those of dielectric capacitors and they exhibit greater power densities and longer cycling ability than conventional rechargeable batteries.[1] Thus, they can be widely used in areas such as mobile electronic devices, camera flash equipment, and back-up power supplies.[2-4] Recently, there has been increased demand for supercapacitors with higher energy densities, better rate capabilities and longer cycling lifetimes for use in newly emerging large scale applications, i.e. hybrid electric vehicles and grid storage.[5] Conventional electrode materials such as carbon,[6-7] transition metal oxides[8-9] and conducting polymers,[10-11] cannot meet these standards due to their low capacitance, high cost and poor stability. Therefore, rapid development of new electrode materials with high performance is essential.

Metal-organic frameworks (MOFs), as a new class of porous materials with an unrivalled degree of tunability, have emerged rapidly in the last years for a wide range of potential applications including catalysis,[12] gas separation,[13] drug delivery,[14-15] imaging and sensing,[16] optoelectronics[17] and energy storage.[18-20] Investigations into the use of MOFs as supercapacitors have expanded in recent years[21-22] and can be classified into two cases. In one case, MOFs are utilized as novel templates for preparing porous metal oxides[23-25] or carbons[26-27] because of their controllable micropore size (0.6-2 nm) and large surface areas. In other case, the MOFs themselves have unique structures incorporating pseudo-capacitive redox centers that can be directly used as a new type

of electrode material. Studies into the direct use of MOFs as supercapacitor electrodes are rarer and more challenging due to the structural flexibility of MOFs.[28] For example, MOFs including Co-,[29-30] Co-Zn-,[31] Zn- and Cd-based materials[32] have been investigated, but only the Co-based MOF exhibited a capacitance of approximately 200 F g^{-1} in LiOH solution.[29] These materials may be considered of limited success due to their poor electrical conductivity, steric hindrance to ion insertion due to the pore size[33-34] and incompatibility between these MOFs and the electrolyte.[28]

To overcome these disadvantages, it is highly desirable to design tailored MOFs materials with unique structures. Tuning of the linker structure may lead to better charge transfer within the framework, while the redox behavior of metal cations inside the MOF could provide a transport pathway for electrons.[28] Thus, MOFs constructed with pathways for facilitating electron transport can solve the problem of insulating character. On the other hand, to eliminate steric limitations by the electrolyte ion with its solvation shell[34] and fully take advantage of the micropores or other channels, MOFs with pores or space sufficiently large to permit quick electrolyte diffusion are desirable. Moreover, active metal cations inside MOFs should be accompanied by matched electrolyte solution in order to ensure the predominant charge storage mechanism can manifest through a pseudocapacitive reaction and thereby exhibit high capacitance.[35]

In the present work, a layered two-dimensional (2D) Ni-based MOF was successfully synthesized and firstly used as a supercapacitor electrode in an aqueous alkaline solution. This material exhibited large capacitance, high-rate capability and cycling stability. The relationships between the intrinsic

characteristics of the Ni-MOF material and its electrochemical properties were investigated in detail.

Experimental

In a typical procedure, 0.166 g of p-benzenedicarboxylic acid (PTA) was dissolved in a 5 ml N, N-dimethylformamide (DMF) with stirring at room temperature. Then, 1.5 mmol of $NiCl_2 \cdot 6H_2O$ (10 ml) was slowly added to the above solution drop by drop. After stirring for 1 h, the mixture was then transformed into a Teflon-lined stainless steel autoclave with a capacity of 35 ml, and was kept at 120 °C for different times. After cooled to room temperature, the resulting precipitate was washed with DMF and alcohol for several times. Finally, the final products were dried at 70 °C for 12 h in air and the Ni-based MOF materials were obtained. Herein, Ni-based MOF materials synthesized for 24 and 12 h are denoted as Ni-MOF-24 and Ni-MOF-12, respectively.

X-ray diffraction (XRD) patterns were recorded on PANalytical X'Pert spectrometer using the Co-Kα radiation and the data were changed to Cu-Kα data. Scanning electron microscopy (SEM) and transmission electron microscopy (TEM) were taken on a Hitachi S4800 instrument and a FEI F20 S-TWIN instrument, respectively. Surface area was determined by Brunauer–Emmet–Teller (BET) method using ASAP2020 from Quanta Chrome. Initially, the sample was vacuum degassed for 6 h at 150℃ under the flow of nitrogen before the BET measurement. Fourier Transform Infrared (FT-IR) transmission spectra were taken on a BRUKER-EQUINOX-55 IR spectrophotometer. Thermo Gravimetric-Differential Thermal Analysis (TG-DTA) was performed using the Setsys Evolution instrumentation with a rate of 10 °C min^{-1} under ambient conditions. X-ray photoelectron spectroscopy (XPS) measurements (ESCALAB 250) were performed to analyze the surface species and their chemical states.

Electrochemical properties of the samples were evaluated in a standard three electrode test pool (Hangzhou Saiao Electrochemistry Technology Co., Ltd). For the working electrode, a mixture containing of 70 wt. % active material, 20 wt. % acetylene black, and 10 wt. % PTFE binder was well mixed. Then the mixture was pressed with several drops of isopropyl alcohol solvent to form a thin sheet. The sheet was rolled to get approximate thickness of 100 μm and then pressed onto a stainless steel mesh. The mass loading of the sample Ni-MOF is about 5 mg cm^{-2}. Platinum foil and saturated calomel electrode were used as the counter and reference electrodes, respectively. The electrolyte was 6 M KOH. Cyclic voltammetry (CV), galvanostatic charge-discharge (GCD) measurements, electrochemical impedance spectroscopy (EIS) were performed on an Electrochemical Workstation (Zahner, IM6). The EIS data was collected with an AC voltage of 10 mV amplitude in the frequency range from 1 MHz to 100 mHz.
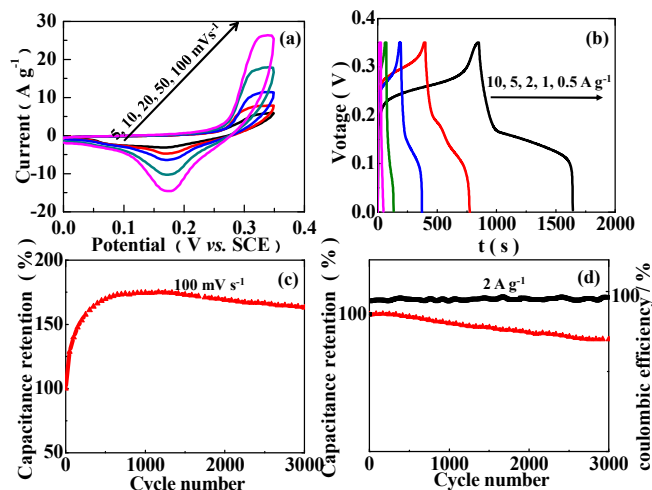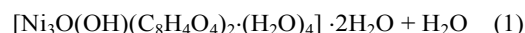
Results and discussion

Fig. 1 Electrochemical performance of the Ni-MOF-24 electrode: (a) CV curves at different scan rates, (b) charge-discharge profiles at different current densities, (c) CV cycling performance, and (d) GCD cycling performance.

Fig. 1 shows the electrochemical performance of Ni-MOF-24 electrode. As depicted in Fig.1a, it clearly exhibits a couple of redox peaks at 0.32 and 0.17 V (*vs*. SCE), indicating that the pseudocapacitive behaviour arised from the surface faradic redox reactions. These peaks may correspond to the intercalation and deintercalation of OH$^-$ during electrochemical reactions based on similar reports for $Ni(OH)_2$.[36-39] This process might be represented by the following equation:

$$[Ni_3(OH)_2(C_8H_4O_4)_2 \cdot (H_2O)_4] \cdot 2H_2O + OH^- - e^- \leftrightarrow$$

$$[Ni_3O(OH)(C_8H_4O_4)_2 \cdot (H_2O)_4] \cdot 2H_2O + H_2O \quad (1)$$

As can be seen from Fig. 1b, a maximum specific capacitance of 1127 F g^{-1} was reached at a rate of 0.5 A g^{-1}. Even at a current density as large as 10 A g^{-1}, the capacitance of 668 F g^{-1} was still retained, indicating that this material had a high rate capability. Accordingly, the maximum power and energy densities were 1750 W kg^{-1} and 19.17 Wh kg^{-1}, respectively. To further investigate the cycling performance, CV and galvanostatic charge-discharge (GCD) tests were executed and the results are shown in Fig. 1c-d. It was found that the capacitance retention was respectively kept at 93% and 91% of its highest value after 3000 cycles, indicating that this kind of Ni-based MOF material not only had large specific capacitance and good rate capability but also had excellent cycling stability. This might be attributed to the fact that the charged transfer resistance was slightly increased after long cycles (Fig. S1).

To date, research to find new materials with excellent electrochemical performance has not yet been successful.[29-32] Lee et al.[29] had successfully used a Co-based MOF as an electrode, but the highest capacitance value measured was only 206 F g^{-1}. Here, our Ni-based MOF material showed a capacitance of 1127 F g^{-1}.To the best of our knowledge, such a capacitance is the highest value in the published reports for

MOFs. The high performance may be attributed to the intrinsic characteristics of the Ni-based MOF material, such as layered structure and favourable exposed facets.
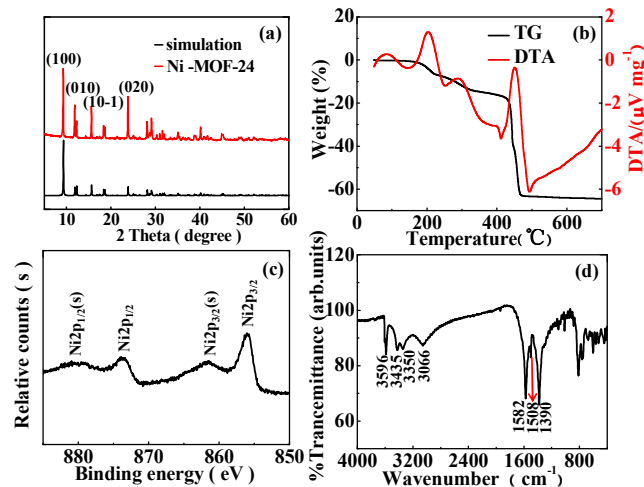

Fig. 2 Characterization results of Ni-MOF-24 material: (a) XRD patterns, (b) TG-DTA curve, (c) XPS, and (d) IR spectrum.

The characterizations of Ni-MOF-24 are depicted in Fig. 2. XRD (Fig. 2a) showed that the diffraction pattern of the synthesized sample was in good agreement with that simulated from the single-crystal data of $[Ni_3(OH)_2(C_8H_4O_4)_2(H_2O)_4]\cdot2H_2O$ (CCDC 638866). The (100) plane of the sample can be identified as the largest exposed facet. TG-DTA curves, shown in Fig. 2b, indicate that initial weight loss of 5.6 % up to 150 °C was due to the loss of two solvated water molecules, which was consistent with the previous report.[40] The weight loss in the range of 170 - 465 °C corresponded to the decomposition of Ni-MOF-24 to yield NiO. XPS analysis, as shown in Fig. 2c, reveals two major peaks centred at around 873.7 and 856.1 eV with a spin-energy separation of 17.6 eV, corresponding to Ni $2p_{1/2}$ and Ni $2p_{3/2}$, respectively, which were characteristic of Ni^{2+} and in good agreement with previous literature reports.[41-42] The two other peaks centred at around 879.6 and 861.1 eV corresponded to Ni $2p_{1/2}$ and Ni $2p_{3/2}$ satellites, respectively, which were also consistent with the reported result for Ni^{2+}.[43] The FTIR spectroscopy of Ni-MOF-24 is shown in Fig. 2d. The bands at $\sim$3596 and 1508 cm^{-1} were respectively attributed to the stretching vibrations of OH^- and *para*-aromatic CH groups. The stretching vibrations of water molecules at around 3435, 3350 and 3066 cm^{-1} indicate that coordinated H_2O molecules are present within the Ni-based material.[44] The strong bands at 1582 and 1390 cm^{-1} were assigned to the asymmetric and symmetric stretching modes of the coordinated (-COO^-) group, respectively. The separation between these two modes indicated that the -COO^- of *p*-BDC is coordinated to Ni *via* a bidentate mode.[45] These results were all in good agreement with the XRD result and further confirmed that the synthesized Ni-based MOF was a kind of nickel hydroxyl-terephthalate-based compound.
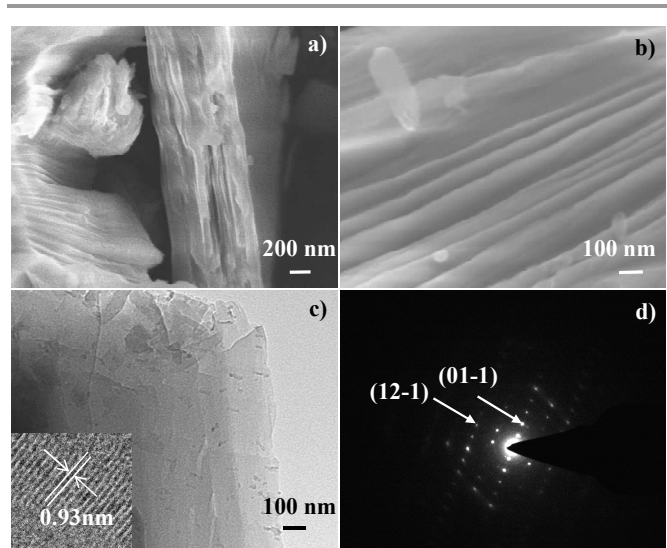

Fig. 3 (a-b) SEM, (c) TEM images (inset is a HRTEM image), and (d) SAED pattern of Ni-MOF-24 sample.

Fig. 3 shows SEM and TEM images of Ni-MOF-24. The images showed that the sample exhibited a loosely packed sheet-like structure. The TEM image in Fig. 3c confirmed that the synthesized product was composed of nanosheets of approximately 10 nm thick. HRTEM in the inset reveals that the lattice fringe was ca. 0.93 nm, corresponding to a d_{100}-spacing, which was in good agreement with the XRD results. The SEAD pattern in Fig. 3d can also be indexed to different planes and <101> zone axis was obtained from the two marked points by the cross-measurement.
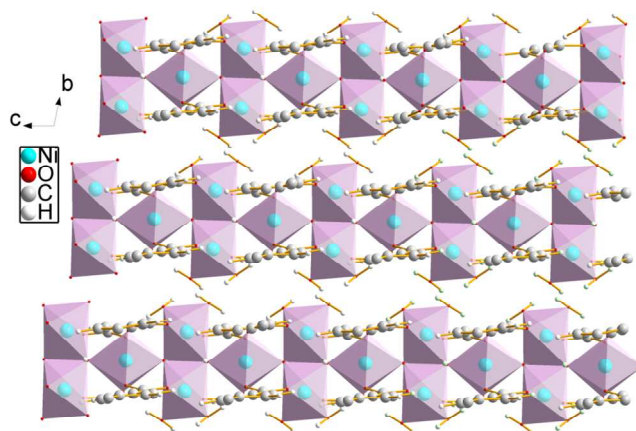

Fig. 4 View of the structure of Ni-MOF-24 along *a* axis.

Fig. 4 shows the view of the Ni-MOF-24 structure along the *a*-axis. The material exhibited a layered structure with infinite layers parallel to the *ac* plane and perpendicular to the *b*-axis. Each layer was built up from one-dimensional (1D) chains of nickel octahedra extended parallel to the c-axis and connected by bridging bidentate tp anions along the *a*-axis. These layers were connected by hydrogen bonds between Ni-coordinated water molecules that ensure cohesion of the

structure. The largest exposed facet of (100) exhibited a perfect structure for the transport of electrons and diffusion of electrolyte solution. Along the *c*-axis, the chains of nickel octahedra with 1D structure connected to other provided a conductive path for electrons, while the parallel layers with interspaces along the *b*-axis promoted the storage and diffusion of electrolyte solution. Such a layered material might exhibit excellent electrochemical performance as an electrode in a supercapacitor.
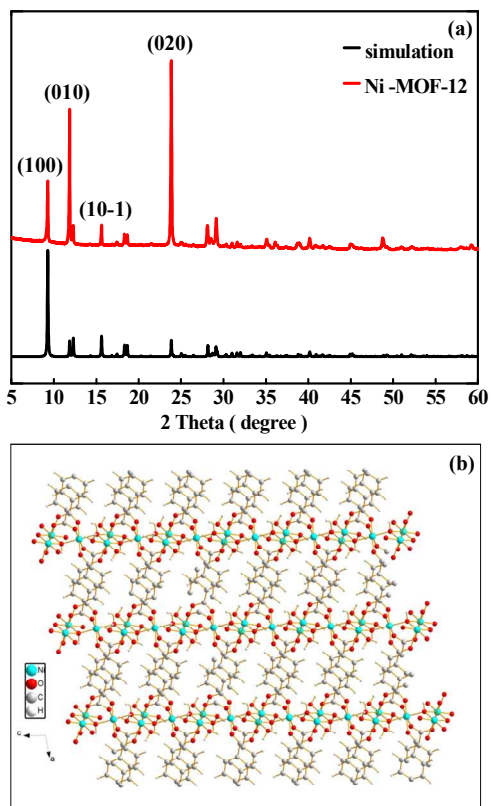

Fig. 5 (a) XRD patterns, and (b) view of the structure along *b* axis of Ni-MOF-12.

To further confirm the effects of the Ni-MOF crystal structure on the electrochemical properties, a sample of Ni-MOF-12 was synthesized over 12 h. By contrast, it was characterized and tested with the same procedures. Fig. 5a shows that this material can be indexed onto a single crystal of $[Ni_3(OH)_2(C_8H_4O_4)_2 (H_2O)_4]\cdot 2H_2O$ (CCDC 638866) with (020) as the largest exposed facet. SAED pattern (Fig, S2) can be indexed to the corresponding planes and the <01-1> zone axis was confirmed. This was in stark contrast to Ni-MOF-24 and its crystal structure is depicted in Fig. 5b. In addition, TG-DTA, XPS, IR and BET measurement results were also presented (Fig.S3-S4). In fact, the difference between Ni-MOF-24 and Ni-MOF-12 was only that they had different exposed facets.

Fig. 6 shows the electrochemical properties of Ni-MOF-24 and Ni-MOF-12. The capacitances of the former are larger than those of the latter at every rate, indicating that the electrode with the largest exposed (100) facet exhibited better performance than that with the largest exposed (020) facets. As
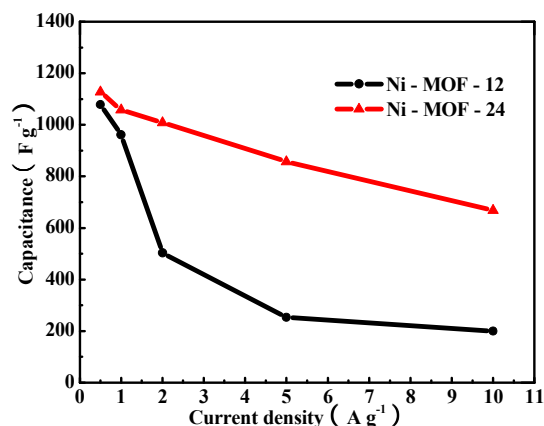

Fig.6 The comparison of specific capacitances at different current densities between the two electrodes.

shown in Fig. 5b, 1-D conductive chains of nickel octahedra still existed along the *c*-axis, which was the same as that of the sample with the largest exposed (100) facet. However, Ni-MOF-12 had no interlayer spaces, micropores or other paths for electrolyte diffusion on (020) facet (Fig. S5). Therefore, Ni-MOF materials with different facets exposed may influence the diffusion of electrolyte and hence may be a key factor in determining their properties.
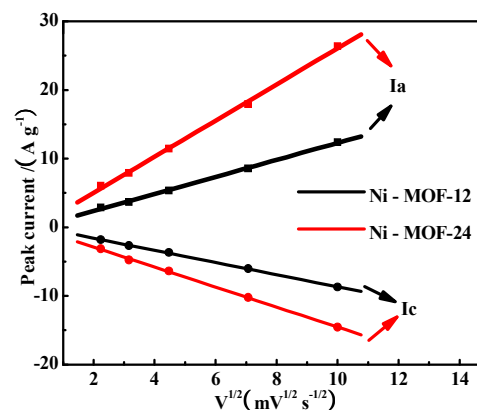

Fig. 7 The relationship between the peak current and sweep rate of the two Ni-based MOF electrodes. (The currents of anode and cathode were abbreviated Ia and Ic, respectively.)

To explore the role of electrolyte diffusion during the pseudocapacitive charge storage process, CV measurements of two electrodes were performed and the relationship between the peak current and the scan rate is presented in Fig.7. Such a relationship can be used to deduce the electrochemical reaction mechanism, including the solid-phase diffusion controlled and surface confined charge-transfer processes.[46-47] In the present work, it was found that the cathodic and anodic peak currents depends linearly on the square root of the scan rates, indicating that the diffusion of electrolyte was dominant in the redox process for Ni-based MOF electrodes. The Ni-MOF materials with different exposed facets influenced the diffusion of electrolyte solution which was a rate controlling step during the

pseudocapacitance storage process. Thus, the Ni-MOF material with the largest exposed (001) facet exhibited a better electrochemical performance.

Conclusions

In summary, a Ni-based layered MOF was firstly used as an electrode material for supercapacitors and exhibited high specific capacitance, good rate capability and cycling stability. A capacitance of 1127 F g^{-1} was achieved and the retention was more than 90% even after 3000 cycles. This excellent electrochemical performance was attributed to the intrinsic characteristics of the Ni-based MOF including its layered structure and favourable exposed facet. The present studies demonstrate that new classed of MOF materials may find applications as supercapacitors in future.

Acknowledgements

Notes and references

[a] State Key Laboratory of Photocatalysis on Energy and Environmet, Fuzhou University, Fuzhou, Fujian 350002, China
[b] Institute of Advanced Energy Materials, Fuzhou University, Fuzhou, Fujian 350002, China

Electronic Supplementary Information (ESI) available: [details of any supplementary information available should be included here]. See DOI: 10.1039/b000000x/

1 P. Simon and Y. Gogotsi, *Nat. Mater.*, 2008, **7**, 845.

2 A. S. Arico, P. Bruce, B. Scrosati, J. M. Tarascon and W. V. Schalkwijk, *Nat. Mater.*, 2005, **4**, 366.

3 V. Subramanian, H. W. Zhu, R. Vajtai, P. M. Ajayan and B. Q. Wei, *J. Phys. Chem. B*, 2005, **109**, 20207.

4 S. Sarangapani, B. V. Tilak and C. P. Chen, *J. Electrochem. Soc.*, 1996, **143**, 3791.

5 G. Huang, F. F. Zhang, L. L. Zhang, X. C. Du, J. W. Wang and L. M. Wang, *J. Mater. Chem. A*, 2014, Advance Article, DOI: 10.1039/C4TA00200H.

6 Q. Li, R. R. Jiang, Y. Q. Dou, Z. X. Wu, T. Huang, D. Feng, J. P. Yang, A. S. Yu and D. Y. Zhao, *Carbon*, 2011, **49**,1248.

7 S. I. Lee, S. Mitani, C. W. Park, S. H. Yoon, Y. Korai and I. Mochida, *J. Power Sources*, 2005, **139**, 379.

8 W. D. Deng, X. B. Ji, Q. Y. Chen and C. E. Banks, *RSC Adv.*, 2011, **1**, 1171.

9 P. Lv, Y. Y. Feng, Y. Li and W. Feng, *J. Power Sources*, 2012, **220**, 160.

10 H. Gao and K. Lian, *J. Power Sources*, 2011, **196**, 8855.

11 H. Gao and K. Lian, *Electrochim. Acta*, 2010, **56**, 122.

12 A. Corma, H. Garcia and F. X. Llabres i Xamena, *Chem. Rev.*, 2010, **110**, 4606.

13 A. U. Czaja, N. Trukhan and U. Mueller, *Chem. Soc. Rev.*, 2009, **38**,1284.

14 P. Horcajada, C. Serre, G. Maurin, N. A. Ramsahye, F. Balas, M. V. Regi, M. Sebban, F. Taulelle and G. Ferey, *J. Am. Chem. Soc.*, 2008, **130**, 6774.

15 G. Ferey, *Chem. Soc. Rev.*, 2008, **37**, 191.

16 P. Horcajada, T. Chalati, C. Serre, B. Gillet, C. Sebrie, T. Baati, J. F. Eubank, D. Heurtaux, P. Clayette, C. Kreuz, J. S. Chang, Y. K. Hwang, V. Marsaud, P. N. Bories, L. Cynober, S. Gil, G. Ferey, P. Couvreur and R. Gref, *Nat. Mater.*, 2010, **9**, 172.

17 L. E. Kreno, K. Leong, O. K. Farha, M. Allendorf, R. P. Van Duyne and J. T. Hupp, *Chem. Rev.*, 2012, **112**, 1105.

18 H. Wu, W. Zhou and T. Yildirim, *J. Am. Chem. Soc.*, 2007, **129**, 5314.

19 N. L. Rosi, J. Eckert, M. Eddaoudi, D. T. Vodak, J. Kim, M. O. Keeffe and O. M. Yaghi, *Science*, 2003, **300**, 1127.

20 F. Vilela, K. Zhang and M. Antonietti, *Energy Environ. Sci.*, 2012, **5**, 7819.

21 H. Y. Shi, B. Deng, S. L. Zhong, L. Wang and A. W. Xu, *J. Mater. Chem.*, 2011, **21**, 12309.

22 A. Almasoudi and R. Mokaya, *J. Mater. Chem.*, 2012, **22**, 146.

23 C. Y. Su, A. M. Goforth, M. D. Smith, P. J. Pellechia and H. C. zurLoye, *J. Am. Chem. Soc.*, 2004, **126**, 3576.

24 X. G. Liu, *Angew. Chem., Int. Ed.*, 2009, **48**, 3018.

25 F. Meng, Z.G. Fang, Z. X. Li, W. W. Xu, M. J. Wang, Y. P. Liu, J. Z, W. R. Wang, D. Y. Zhao and X. H. Guo, *J. Mater. Chem. A*, 2013, **1**, 7235.

26 H. L. Jiang, B. Liu, Y. Q. Lan, K. Kuratani, T. Akita, H. Shioyama, F. Zong and Q. Xu, *J. Am. Chem. Soc.*, 2011, **133**, 11854.

27 A. J. Amali, J. K. Sun and Q. Xu, *Chem. Commun.*, 2014, **50**, 1519.

28 A. Morozan and F. jaouen, *Energy Environ. Sci.*, 2012, **5**, 9269.

29 D. Y. Lee, S. J. Yoon, N. K. Shrestha, S. H. Lee, H. Ahn and S. H. Han, *Microporous Mesoporous Mater.*, 2012, **153**, 163.

30 D. Y. Lee, D. V. Shinde, E. K. Kim, W. Lee, I. W. Oh, N. K. Shrestha, J. K. Lee and S. H. Han, *Microporous Mesoporous Mater.*, 2013, **171**, 53.

31 R. Diaz, M. Gisela Orcajo, J. A. Botas, G. Calleja and J. Palma, *Mater. Lett.*, 2012, **68**, 126.

32 Y. Gong, J. Li, P. G. Jiang, Q. F. Li and J. H. Lin, *Dalton Trans.*, 2013, **42**, 1603.

33 G. Combarieu, M. Morcrette, F. Millange, N. Guillou, J. Cabana, C. Grey, I. Margiolaki, G. Ferey and J. M. Tarascon, *Chem. Mater.*, 2009, **21**,1602.

34 A. Fateeva, P. Horcajada, T. Devic, C. Serre, J. Marrot, J. M. Grenèche, M. Morcrette, J. M. Tarascon, G. Maurin and G. Ferey, *Eur. J. Inorg. Chem.*, 2010, **24**, 3789.

35 J. E. Halls, D. M. Jiang, A. D. Burrows, M. A. Kulandainathanb and F. Marken, *Electrochemistry*, 2013, **12**, 187.

36 N. A. Alhebshi, R. B. Rakhi and H. N. Alshareef, *J. Mater. Chem. A*, 2013, **1**, 14897.

37 H. J. Yan, J. W. Bai, J. Wang, X. Y. Zhang, B. Wang, Q. Liu and L. H. Liu, *Cryst. Eng. Comm.*, 2013, **15**, 10007.

38 H. Wang, Y. Liang, T. Mirfakhrai, Z. Chen, H. S. Casalongue and H. Dai, *Nano Res.*, 2011, **4**, 729.

39 G. S. Gund, D. P. Dubal, S. B. Jambure, S. S. Shinde and C. D. Lokhande, *J. Mater. Chem. A*, 2013, **1**, 4793.

40 A. Carton, A. Mesbah, T. Mazet, F. Porcher and M. F. ois, *Solid State Sciences*, 2007, **9**, 465.

41 J. W. Lee, T. Ahn, D. Soundararajan, J. M. Ko and J. D. Kim, *Chem. Commun.*, 2011, **47**, 6305.

42 J. Liang, R. Ma, N. Iyi, Y. Ebina, K. Takada and T. Sasaki, *Chem. Mater.*, 2010, **22**, 371.

43 H. Yan, J. Bai, J.Wang, X. Zhang, B. Wang, Q.Liu and L. Liu, *CrystEngComm*, 2013, **15**, 10007.

44 F. Zhang, L. Hao, L. J. Zhang and X. G. Zhang, *Int. J. Electrochem. Sci.*, 2011, **6**, 2943.

45 A. Mesbah, P. Rabu, R. Sibille, S. b. Lebegue, T. Mazet, B. Malaman and M. Francois, *Inorg. Chem.*, 2014, **53**, 872.

46 Y. Wang, Z. Hong, M. Wei and Y. Xia, *Adv. Funct. Mater.*, 2012, **22**, 5185.

47 J. T. Zhang, S. Liu, G. L. Pan, G. R. Li and X. P. Gao, *J. Mater. Chem. A*, 2014, **2**, 1524.

Journal of Materials Chemistry A Accepted Manuscript

TOC
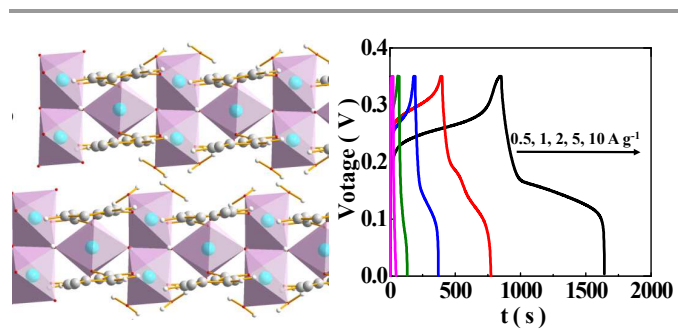
Layered structure Ni-based MOF was firstly used as the electrode material for a supercapacitor and exhibited a large specific capacitance of 1127 F g^{-1} at 0.5 A g^{-1}.